Fifth International Conference on CFD in the Process Industries
CSIRO, Melbourne, Australia
13-15 December 2006

A CFD STUDY OF THE BUBBLE DEFORMATION DURING DETACHMENT

Anh BUI and Richard MANASSEH

CSIRO Manufacturing & Materials Technology, Highett, Victoria 3190, AUSTRALIA

ABSTRACT

In this work, a numerical model of immiscible multiphase flows with interfaces has been developed. The flow of compressible gas and nearly incompressible fluid has been described by a single set of the Navier-Stokes equations with a generic equation of state used for both phases. By employing the level set front-capturing method, a sharp liquid-gas interface could be maintained. The proposed numerical model has been used to investigate some multiphase problems with the deformation of the gas-liquid interface involved. The computational results were validated against theoretical analyses and experimental data. In a simulation of bubble detachment and the related sound emission, the relation between the bubble deformation and the acoustic signal generation was predicted by the model which corresponded well with the available experimental data.

NOMENCLATURE

c	sound speed
e	specific internal energy
F	force
H	Heaviside function
p	pressure
p_∞	fluid stiffness parameter
t	time
u	velocity
δ	Delta function
ε	regularization parameter
ϕ	level function
γ	effective ratio of specific heats
μ	dynamic viscosity
ρ	density
σ	surface tension coefficient

INTRODUCTION

When bubbles detach from a pipe or orifice they often deform greatly and oscillate volumetrically, which in turn emits sound at a certain frequency characterised by the bubble detachment radius and the ambient pressure. Bubble detachment happens in many natural and technological processes such as nucleate boiling or gas sparging, which have applications in food and minerals processing, biotechnology, medicine and oceanography. As reported in the experimental and numerical studies by Mitrovic (1997) and Manasseh et al. (1998, 2001a,b) the bubble detachment process is characterized by the formation, contraction and break-off of the neck joining the growing bubble and its parent body of gas. The process is governed by the actions of gravity, viscosity, inertia and surface tension. As a bubble breaks off, its neck retracts quickly, resulting in an inrush of liquid that penetrates the bubble. A jet is formed when the surface tension is not enough to counter the inertia of the accelerated liquid. In the works by Manasseh et al. (1998, 2001a,b) bubble detachment and the associated jet formation were found to generate a distinctive acoustic signal, which can be used to identify the current stage of the bubble detachment process and bubble shape.

The CFD modelling of gas-liquid flows with interfaces is a complex task due to the complex deformation of the interface and steep change of fluid properties across it. There are two different approaches to the modelling of multiphase flows using fixed Eulerian meshes. In the multifluid method, each fluid phase is described by a separate set of the conservation equations and the interface between the fluids is not directly modelled. The interfacial effect in coupling the fluids is represented by various surface-averaged interfacial forces and heat-mass transfers between phases. The multifluid method requires that information about interfacial topology is predetermined. Another method for multiphase flow modelling is based on the assumption that the whole flow field comprising different fluid phases can be described as a single fluid with spatially varying properties. In this method, the evolution of the phase interface in time is modelled directly by front-tracking methods, such as the Marker in Cell (MAC), the Volume-of-Fluid (VOF) or the level-set methods. The problem of bubble detachment has been numerically investigated in the work by Manasseh et al. (1998) using of the VOF method, in which the interface is described by a fractional volume function. The level set method which was first introduced by Osher et al. (1988) uses a level function which is continuous across the interface. The interface is defined as the zero level of that function.

A numerical study of bubble detachment has been conducted in this work with use of the single-fluid formulation of the gas-liquid flow. By employing the level set front-capturing method, a sharp liquid-gas interface could be maintained during the simulation.

MODEL DESCRIPTION

The model is based on: i) the level-set method to track the interfaces; and (ii) an explicit flow solver for compressible and nearly incompressible multiphase flows. Coupled with high-resolution advection schemes, this modelling approach would allow the description of the movement of gas and fluid and the deformation of the interface separating them on a fixed computational mesh.

Description of the compressible-nearly incompressible multiphase flow

The flow of compressible-nearly compressible multiphase flow is described by a single set of the Navier-Stokes equations as follows:

$$\begin{aligned} &\frac{\partial \rho}{\partial t} + \vec{u}\nabla\rho + \rho\nabla\vec{u} = 0 \\ &\rho\left(\frac{\partial \vec{u}}{\partial t} + \vec{u}\cdot\nabla\vec{u}\right) = -\nabla p + \nabla\left(\mu\nabla\vec{u}\right) + \vec{F}_s + \vec{F}_b \end{aligned} \tag{1}$$

where F_s and F_b are the surface tension force and body force, respectively.

Assuming that the thermodynamic properties of both the compressible and nearly-incompressible fluids are governed by a generic equation of state (EOS):

$$\rho e = \frac{p + \gamma p_\infty}{\gamma - 1}, \tag{2}$$

where p_∞ is a stiffness parameter and γ is the ratio of specific heats, an additional differential equation for the pressure can be derived from the mass and energy conservation equations as:

$$\frac{\partial p}{\partial t} + \vec{u}\nabla p = -\rho c^2 \nabla\vec{u} \tag{3}$$

where c is the sound speed which is defined as:

$$c^2 = \gamma\left(\frac{p + p_\infty}{\rho}\right) \tag{4}$$

The use of the pressure evolution equation (3) and the model based on the primitive variables *(ρ, u, p)* in which the relative amounts of gas and liquid are not conserved is one of the methods used to reduce the problem of pressure oscillations at the interface which is inherent in the conservative multifluid models (see Abgrall et al. (2001)).

The Level-Set Front-Capturing Method

Essentially, the level-set method employs a *smooth* level function, ϕ, to describe the interface separating two immiscible fluids (Osher et al. (1988)). This level function is chosen as a signed distance function with the zero level set defining the interface location. The level function is positive in one fluid region and negative in the other one and its absolute value indicates the distance to the interface. The level function is convected by flow field $\vec{u}$ as follows:

$$\phi_t + (\vec{u}\cdot\nabla)\phi = 0 \tag{5}$$

Since this function is smooth across the interface (unlike the fluid properties) the above convection equation can be solved with high-order accuracy and without introducing numerical oscillations. Using the level function, the steep changes of fluid properties across the interface can be smoothed out to minimize numerical oscillations in the solution of Navier-Stokes equations as follows:

$$\begin{aligned} \rho_\varepsilon &= \rho_1 + (\rho_2 - \rho_1)\cdot H_\varepsilon(\phi), \\ \mu_\varepsilon &= \mu_1 + (\mu_2 - \mu_1)\cdot H_\varepsilon(\phi), \end{aligned} \tag{6}$$

where H_ε is a regularization Heaviside function and ε is a regularization parameter:

$$H_\varepsilon(d) = \begin{cases} 0 & \text{if } d < \varepsilon, \\ (d+\varepsilon)/(2\varepsilon) + \sin(\pi d/\varepsilon)/(2\pi) & \text{if } |d| \le \varepsilon, \\ 1 & \text{if } d > \varepsilon. \end{cases} \tag{7}$$

Another major advantage of using the level function is that the geometric properties of the interface can also be easily determined:

Normal vector:

$$\vec{\mathbf{n}} = \frac{\nabla\phi}{|\nabla\phi|}, \tag{8}$$

Surface curvature:

$$\kappa = \nabla\vec{\mathbf{n}} = \nabla\cdot\frac{\nabla\phi}{|\nabla\phi|}. \tag{9}$$

The surface tension force appearing in the momentum equations can be defined in terms of the level function (Sussman et al. (2000)) as:

$$\vec{F}_s = \sigma\kappa\delta(\phi)\vec{\mathbf{n}} = \sigma\delta_\varepsilon(\phi)\cdot\nabla\phi\cdot\nabla\left(\frac{\nabla\phi}{|\nabla\phi|}\right), \tag{10}$$

where σ is the surface tension coefficient and $\delta_\varepsilon(\phi)$ is a delta function corresponding to H_ε:

$$\delta_\varepsilon(\phi) = \begin{cases} 0 & \text{if } |\phi| > \varepsilon, \\ \frac{1}{2}(1+\cos(\frac{\pi\phi}{\varepsilon}))/\varepsilon & \text{if } |\phi| \le \varepsilon. \end{cases} \tag{11}$$

The level set method can handle complex topological changes of the interface, such as breaking or merging, and its formulation is generic for two- and three-dimensional problems.

During the long evolvement of the level function it is important to keep it as a signed distance to the interface so that the interface curvature can be correctly evaluated. Therefore, a level-set 're-initialization' procedure is necessary in which a Hamilton-Jacobi equation of the form:

$$\phi_\tau + sign(\phi)\left(|\nabla\phi| - 1\right) = 0 \tag{12}$$

is solved iteratively until convergence. This procedure will reinitialize the level function back to the signed-distance one, i.e. satisfying $|\nabla\phi|=1$, without disturbing the location of the interface. Normally, it is sufficient to do this procedure occasionally and just for a narrow band around the interface.

Improvement of the Level-Set Method

The level set method while having many advantages compared to other front-capturing methods still has problem with mass conservation, especially when the interface undergoes severe deformation. A remedy to this problem has been proposed by Sussman et al. (2000), in which the level set method is coupled with the volume-of-fluid (VOF) method. The coupled method (named CLSVOF) is based on a VOF function which can be convected accurately so that mass is conserved while using the level function to evaluate the interface geometric and phase properties.

NUMERICAL METHOD

The system of differential equations (1), (3) and (5) can be solved using the numerical procedure proposed in the work by Yoon et al. (1999), which consists of two stages:

Advection stage:

$$\begin{cases} \dfrac{\rho^* - \rho^n}{\Delta t} + \vec{u}^n \nabla \rho^n = 0 \\ \dfrac{\vec{u}^* - \vec{u}^n}{\Delta t} + \vec{u}^n \nabla \vec{u}^n = 0 \\ \dfrac{p^* - p^n}{\Delta t} + \vec{u}^n \nabla p^n = 0 \\ \dfrac{\phi^* - \phi^n}{\Delta t} + \vec{u}^n \nabla \phi^n = 0 \end{cases}, \qquad (13)$$

High-resolution numerical schemes such as ENO (Essentially-Non-Oscillatory), Weighted ENO (WENO), and Optimized WENO (OWENO) (see Wang et al. (2001)) have been tested for convective term discretization.

Non-advection stage:

$$\begin{cases} \dfrac{\rho^{n+1} - \rho^*}{\Delta t} = -\rho^* \nabla \vec{u}^{n+1} \\ \dfrac{\vec{u}^{n+1} - \vec{u}^*}{\Delta t} = -\dfrac{1}{\rho^*} \nabla p^{n+1} + \nabla\left(\mu \nabla \vec{u}^*\right) + \vec{F}_s(\phi^*) + \vec{F}_b \\ \dfrac{p^{n+1} - p^*}{\Delta t} = -\rho^* c^2 \nabla \vec{u}^{n+1} \\ \phi^{n+1} = \phi^* \end{cases} \qquad (14)$$

The equation system (14) is solved using the predictor-corrector method (Yoon et al. (1999)). In the predictor step, an intermediate evaluation of velocities, u^{**}, is obtained as in (14) with the intermediate pressure p^* used instead of p^{n+1}. In the corrector step, a pressure correction equation of the form:

$$\nabla\left(\frac{1}{\rho^*} \cdot \nabla \delta p\right) = \frac{\delta p}{\Delta t^2 \gamma\left(p^* + p_\infty\right)} + \frac{\nabla \vec{u}^{**}}{\Delta t} \qquad (15)$$

is solved using an iterative Generalized Minimum Residual (GMRES) solver. The pressure correction obtained from (15) is then used to update density, velocities and pressure as follows:

$$\begin{cases} \rho^{n+1} = \rho^*(1 - \Delta t \nabla \vec{u}^{n+1}) \\ \vec{u}^{n+1} = \vec{u}^{**} - \dfrac{\Delta t}{\rho^*} \nabla \delta p \\ p^{n+1} = p^* + \delta p \end{cases} \qquad (16)$$

COMPUTATIONAL RESULTS AND DISCUSSIONS

The level set front-capturing method was tested on the modelling of the two-dimensional solid-body rotation of a shape (Figure 1) inside a square box of unit size. This shape was first introduced by Zalesak (1979) to study the accuracy of the advection algorithms. The simulation was conducted on a 100x100 uniform computational mesh with the ENO numerical scheme used. The notched circle of 0.3 units in diameter did one rotation around the centre at (0.5, 0.5) in 1000 time steps. The regularization parameter ε was one and a half of the control volume size. The initial and final shapes are both shown in Figure 1. While both the level set and CLSVOF gave reasonable predictions of the shape at the end of the rotation, much better conservation of the volume was obtained with the CLSVOF method.

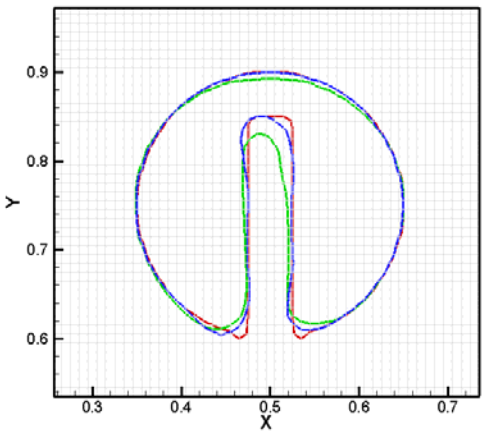

Figure 1: Rotation of a shape – Red line: initial shape; green line: level set result; blue line: CLSVOF result.

An additional simulation test was conducted for the problem of bubble bursting. Bursting of a gas bubble at the gas-liquid surface has been numerically investigated in the past (see Duchemin et al. (2002)). In this work, the simulation of bubble bursting was conducted on a 2D axisymmetric computational domain. The interface curvature is defined from the level function as:

$$\kappa = \frac{\phi_r^2 \phi_{zz} + \phi_z^2 \phi_{rr} - 2\phi_r \phi_z \phi_{rz} + \phi_r\left(\phi_r^2 + \phi_z^2\right)/r}{\left(\phi_r^2 + \phi_z^2\right)^{1.5}} \qquad (17)$$

where r and z indicate the radial and axial coordinates, respectively.

The computational domain size was 6 x 24 mm which was discretized by a uniform mesh of 96 x 192. The initial bubble was 4 mm in diameter and located just below the gas-liquid interface as shown in Figure 3. The gas and liquid densities were 1 kg/m^3 and 1000 kg/m^3, respectively. Both gas and liquid were assumed to be nearly incompressible with γ = 7.15 and $p_\infty = 3.05 \cdot 10^8$ Pa. The surface tension coefficient was 0.051 kg/s^2 and the dynamics viscosities of liquid and gas were $4.728 \cdot 10^{-3}$ and $4.728 \cdot 10^{-5}$ Pa s, respectively. Since the initial bubble radius was much bigger than the viscous-capillary length, $R_v = \mu_l^2/(\rho_l \sigma)$ the effect of viscosity was expected to be negligible compared to the capillary effect.

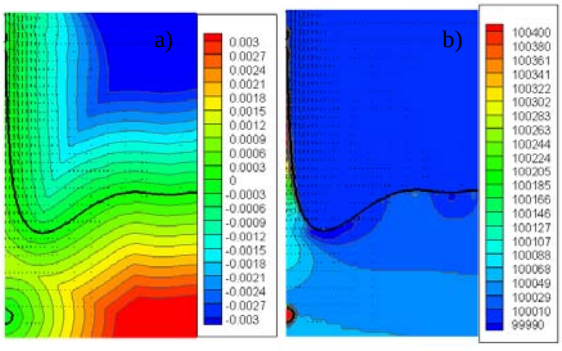

Figure 2: Distributions of the level set function and pressure at 7.13ms.

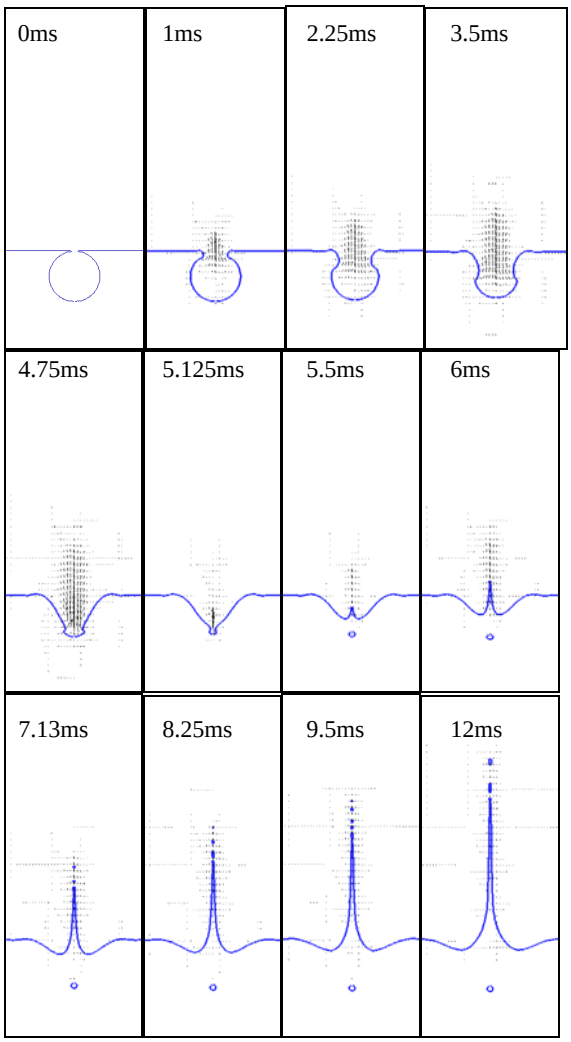

Figure 3: Formation of a jet due to bubble bursting.

The simulation results are shown in Figures 2-3. The concept of the level set front-capturing is illustrated in Figure 2a where the level function isolines are displayed together with the thick line showing the gas-liquid interface (VOF function equal to 0.5). The reinitialization procedure is seen to keep the level function around the interface to be the signed distance. The predictions of the collapse of the initial gas bubble and formation of a liquid jet are presented in Figure 3. Entrapment of gas and creation of a small gas bubble before the jet formation can be seen at approximately 5.125ms. Some explanation for bubble entrapment during bubble bursting at a free surface can be found in the work by Duchemin et al. (2002). Excellent conservation of the entrapped bubble volume was achieved (see Figure 3) despite the relatively coarse computational mesh used. The jet formation was followed by the creation of liquid droplets which detached from the jet due to the interface instability. These droplets were small and could not adequately be resolved with the used grid size. The calculated jet speed at the time of the first droplet detachment is about 4.4m/s, which is in good agreement with the results reported in the work by Duchemin et al. (2002).

Simulation of bubble detachment was also conducted in the axisymmetric coordinate system. The computational domain size was 19 x 13 mm (see Figure 6) described by a uniform 768 x 512 computational mesh. The bubble density and viscosity were set as 1.2 kg/m^3 and 1.7·10^{-5} Pa s. The liquid density and viscosity had their usual physical values of 1000 kg/m^3 and 0.001 Pa s. The bubble was assumed to be filled with an ideal gas with γ = 1.4 and p_∞ = 0 Pa and the liquid was assumed to be nearly incompressible with γ = 7.15 and p_∞ = 3.05·10^8 Pa. The surface tension coefficient was that of the air-water interface, i.e. 0.074 kg/s^2. Other parameters and conditions were chosen to match the experiment described in the papers by Manasseh et al. (1998, 2001). In the simulation, the bubble was initialized as a sphere attached to a cylinder (Figure 6). The relative pressure (p-p_{env}) was monitored at points A and B.

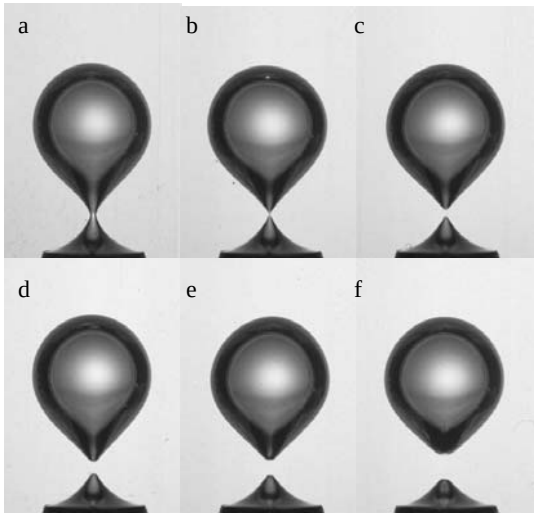

Figure 4: Experimental observation of bubble detachment and jet formation (Manasseh et al., (1998, 2001)).

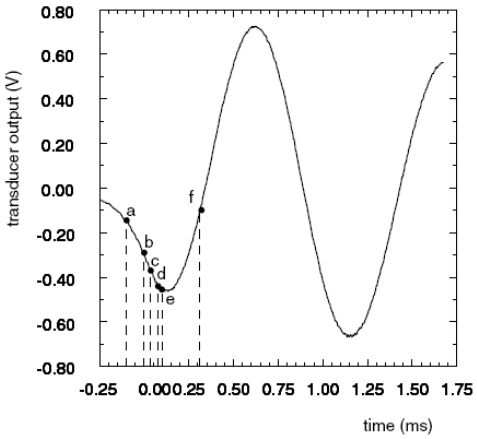

Figure 5: The measured acoustic signal (Manasseh et al., (1998, 2001b)). A decrease of the transducer voltage indicates an increase of the acoustic pressure and 1V corresponds to approximately 100 Pa.

The simulation results are shown in Figures 7-10. As seen in Figures 7 and 9, pressure builds up significantly around the bubble neck prior to the bubble detachment. This build-up of pressure is caused by the surface tension action as described in the work by Mitrovic (1997) when the pressure difference between gas and liquid, defined by

$$\Delta p = p_g - p_l = \sigma\left(\frac{1}{r} - \frac{1}{R}\right)$$

where r is the radius of the narrowest cross-section of the bubble neck and R is the curvature of the bubble neck in the r-z plane, increases greatly as r approaches zero.

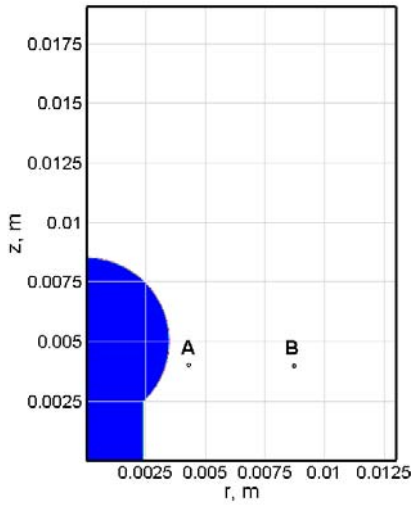

Figure 6: Computational domain and initial bubble shape. Points A and B are the places where pressure was monitored.

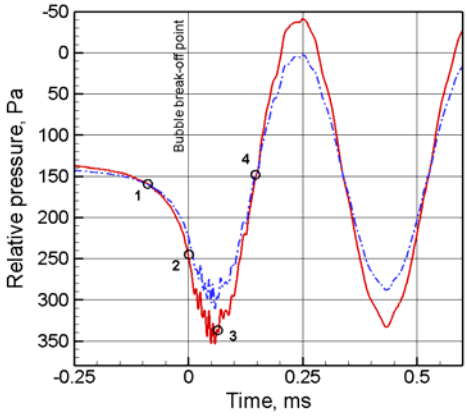

Figure 7: Predictions of relative pressure change in time at point A (solid line) and point B (dot-dashed line).

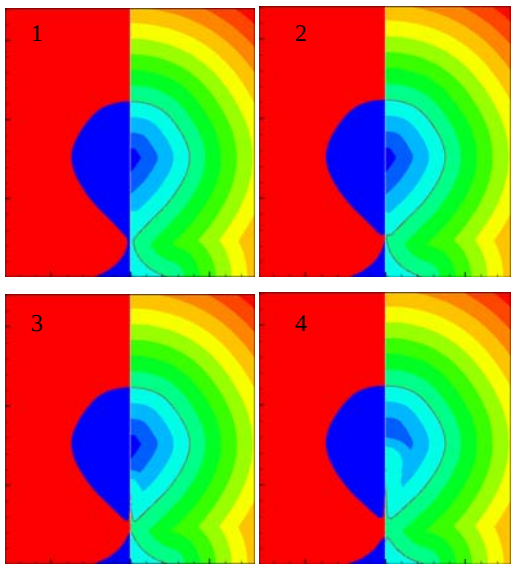

Figure 8: Contours of VOF (left) and level set (right) functions at times given in Figure 7.

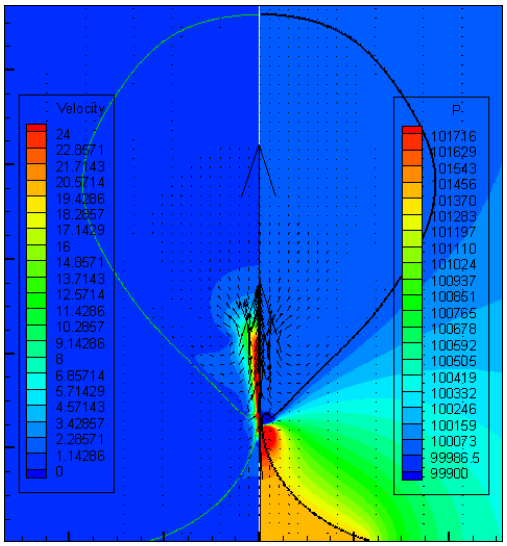

Figure 9: Close-up of pressure distribution and flow field at bubble break-off (point 2 in Figure 7).

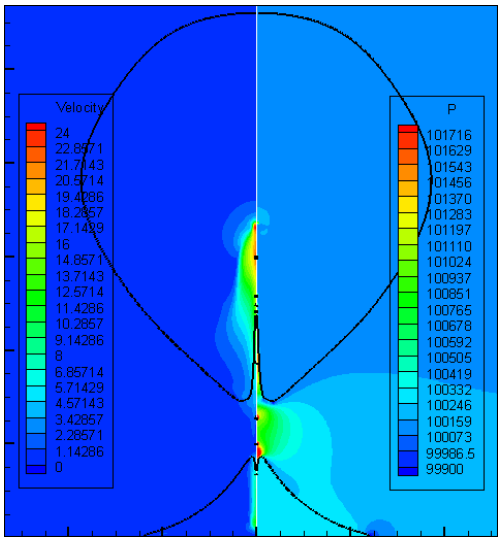

Figure 10: Close-up of pressure and velocity distributions at point 4 in Figure 7.

The predicted shapes of the bubble at different times before and after bubble detachment (Figure 8) are qualitatively comparable to the experimental observation by Manasseh et al. (1998, 2001) (Figure 4). The formation of a liquid jet penetrating the bubble (caused by the retraction of the broken bubble neck) was also predicted (Figures 8 and 10), which was explained in the work of Mitrovich (1997) and confirmed by Manasseh et al. (1998, 2001) (Figure 4). A partner jet going backward to the nozzle was also seen in the simulation results (Figure 10) and can also be observed in experiments. The relation between the bubble deformation and the acoustic signal generated during the process of bubble detachment was obtained from the simulation (shown in Figures 7 and 8), which corresponds well with the experimental data (shown in Figures 4 and 5). The calculated and experimental pressure amplitude were of the same order of magnitude. However, the frequency of pressure oscillation resulted from the bubble detachment was overpredicted in this work compared to the corresponding experimental data (Manasseh et al. (1998, 2001)). As explained in the Appendix below, the limited size of the computational

domain and the applied boundary conditions could greatly affect the oscillation frequency of the bubble.

CONCLUSION

In this work, a numerical model of immiscible multiphase flows with interfaces has been developed. The flow of compressible gas and nearly incompressible fluid has been described by a single set of the Navier-Stokes equations with a generic equation of state used for both phases. The liquid-gas interface has been tracked explicitly and kept sharp by the level set front-capturing method. The model has been tested in simulations of bubble bursting and bubble detachment problems and was found to be able to provide reasonable predictions of the gas-liquid interface deformation with minimal numerical diffusion and volume loss. The simulation tests indicated that the proposed numerical method was capable of dealing with multiphase flows with variable compressibility and big differences in the phase properties. In a simulation of bubble detachment and the related sound emission, the relation between the bubble deformation and the acoustic signal generation was predicted by the model which corresponded well with the available experimental data.

REFERENCES

ABGRALL, R., and KARNI, S., (2001), "Computations of compressible multifluids", *J. Comp. Phys*., **169**, 594-623.

OSHER, S., and SETHIAN, J.A., (1988), "Fronts propagating with curvature-dependent speed: algorithms based on Hamilton-Jacobi formulations", *J. Comp. Phys*., **79**, 12-49.

SUSSMAN, M., and PUCKETT, E.G., (2000), "A coupled level set and volume-of-fluid method for computing 3D and axisymmetric incompressible two-phase flows", *J. Comp. Phys.,* **162**, 301-337.

YOON, S.Y. and YABE, T., (1999), "The unified simulation for incompressible and compressible flow by the predictor-corrector scheme based on the CIP method", *Computer Phys. Communications,* **119**, 149-158.

WANG, Z.J., and CHEN, R.F., (2001) "Optimized Weighted Essentially Non-Oscillatory Schemes for linear waves with discontinuity", *J. Comp. Phys*., **174**, 381-404.

ZALESAK, S.T., (1979), "Fully multidimensional flux-corrected transport algorithms for fluids", *J. Comp. Phys.*, **31**, 335-362.

DUCHEMIN, L., POPINET, S., ZOSSERAND, C., and ZALESKI, S., (2002), "Jet formation in bubbles bursting at free surface", *Phys. Fluids*, 14, 3000-3008.

MANASSEH, R., LAFONTAINE, R.F., DAVY, J., SHEPHERD, I.C., ZHU, Y, (2001a), "Passive acoustic bubble sizing in sparged systems", *Exp. Fluids,* 30(6), 672-682.

MANASSEH, R., BUI, A., SANDERCOCK, J., and OOI, A., (2001b), "Sound Emission Processes on Bubble Detachment", *Proceedings of 14th Australian Fluid Mech. Conf., Adelaide*.

MANASSEH, R., YOSHIDA, S., and RUDMAN, M., (1998), "Bubble formation processes and bubble acoustic signals", *Proceedings of 3rd Int. Conf. on Multiphase Flows, Lyon, France.*

MITROVIC, J., (1997), "Formation of a liquid jet after detachment of a vapour bubble", *Int. J. Heat Mass Transfer,* **40**, 4309-4317.

LEIGHTON, T.G., and WALTON, A.J., (1987), "An experimental study of the sound emitted from gas bubbles in a liquid", *Eur. J. Phys*., **8**, 98-104.

APPENDIX

Following the work by Leighton et al. (1987) the oscillation frequency of a bubble confined in cylindrical domain can be determined. A bubble of radius *a* located near the bottom of a cylindrical domain (Figure 11) is considered.

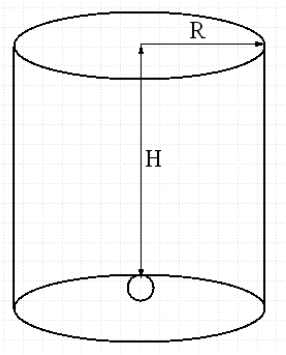

Figure 11: Bubble in a confined cylindrical domain.

Assuming that the bubble of volume V oscillates with amplitude A_o and frequency f and the gas within the bubble to obey the law $p_g V^{\gamma}$ = constant, the maximum work done in compressing the bubble is $6\pi\gamma p_o a A_o^2$, where p_o is the pressure of the surrounding liquid. Assuming that the domain is confined by the bottom and cylindrical impenetratable walls and the fluid can only moves through the top domain surface, the work generated by bubble oscillation is transferred to the motion of the liquid column of height H with the kinetic energy of this column defined by:

$$E = \frac{1}{2}\rho H \pi R^2 v^2$$

where v is the velocity of the column motion. Assuming that the liquid is incompressible, v is related to the bubble oscillation as follows:

$$\pi R^2 v = 4\pi a \dot{a} .$$

Equating the maximum work by the bubble to the maximum kinetic energy of the liquid gives:

$$(2\pi f)^2 = \frac{3}{4}\frac{R^2}{H}\frac{\gamma p_o}{\rho a^3}$$

or

$$f = \frac{1}{2\pi}\sqrt{\frac{3\gamma p_o}{\rho a^2}} \cdot \sqrt{\frac{R^2}{4aH}} .$$

The above formulation of the frequency of the bubble oscillation is similar to that obtained for a bubble oscillating in an infinite volume of liquid (Leighton et al. (1987)) with the effects of domain sizes and confinement accounted for by the last term.